



Regulation of biomaterial implantation-induced fibrin deposition to immunological functions of dendritic cells

Wenhui Hu^{a,b,1}, Yun Wang^{a,b,1}, Jin Chen^{a,b,1}, Peng Yu^{a,b}, Fuzhou Tang^{a,b}, Zuquan Hu^{a,b},
Jing Zhou^{a,b}, Lina Liu^{a,b}, Wei Qiu^{a,b}, Yuannong Ye^{a,b}, Yi Jia^{a,b}, Shi Zhou^{d,**}, Jinhua Long^{c,***},
Zhu Zeng^{a,b,e,f,*}

^a School of Basic Medical Sciences / School of Biology & Engineering, Guizhou Medical University, Guiyang, 550025, PR China

^b Key Laboratory of Infectious Immunity and Antibody Engineering in Guizhou Province, Guiyang, 550025, PR China

^c Department of Head & Neck, Affiliated Tumor Hospital of Guizhou Medical University, Guiyang, 550004, PR China

^d Department of Interventional Radiology, Affiliated Hospital of Guizhou Medical University, Guiyang, 550004, PR China

^e Key Laboratory of Endemic and Ethnic Diseases, Ministry of Education, Guizhou Medical University, Guiyang 550004, Guizhou, PR China

^f State Key Laboratory of Functions & Applications of Medicinal Plants, Guizhou Medical University, Guiyang, 550004, PR China

ARTICLE INFO

Keywords:

Biomaterial implantation
Fibrin
Dendritic cells
Immunological functions
Biomechanics
Mechanobiology

ABSTRACT

The performance of implanted biomaterials is largely determined by their interaction with the host immune system. As a fibrous-like 3D network, fibrin matrix formed at the interfaces of tissue and material, whose effects on dendritic cells (DCs) remain unknown. Here, a bone plates implantation model was developed to evaluate the fibrin matrix deposition and DCs recruitment *in vivo*. The DCs responses to fibrin matrix were further analyzed by a 2D and 3D fibrin matrix model *in vitro*. *In vivo* results indicated that large amount of fibrin matrix deposited on the interface between the tissue and bone plates, where DCs were recruited. Subsequent *in vitro* testing denoted that DCs underwent significant shape deformation and cytoskeleton reorganization, as well as mechanical property alteration. Furthermore, the immune function of imDCs and mDCs were negatively and positively regulated, respectively. The underlying mechano-immunology coupling mechanisms involved RhoA and CDC42 signaling pathways. These results suggested that fibrin plays a key role in regulating DCs immunological behaviors, providing a valuable immunomodulatory strategy for tissue healing, regeneration and implantation.

1. Introduction

Biomaterial implantation is increasingly important in the practice of clinical therapy [1–3], an appropriate host response to biomaterials turns out to be largely determined the performances and the therapeutic effects of these implants *in vivo* [4,5]. After implantation, fibrin as the main components of provisional matrix, which immediately formed at the interface of tissue and material, and plays an important role in hemostatic and serves as scaffold for following host immune cells in the subsequent events of the cellular immune response [6,7]. Although numerous studies have focused on the effects of the material itself such as the biomaterial composition [3,8,9], surface roughness [10] and spatial structure [11] on the behaviors of immune cells, however, the response of immune cells on

the provisional matrix fibrin which acts as an outer coverings layer at the surface of biomaterial remains largely unknown.

Biomaterial implantation usually initiates a series of host immune responses, starting with hemostasis, inflammatory responses and tissue regeneration [2]. Fibrin as the key step of the coagulation cascade, assembled rapidly and occurs almost within minutes and lasts for a few days to a week depending on the nature and site of the implants [2,12]. Fibrin formed by the polymerization of their soluble precursor fibrinogen in blood, and this process is initiated by the protease thrombin, which is activated in response to injury or implantation [2,6]. Following initial blood/material interactions and provisional matrix fibrin formation, acute and chronic inflammation occurs sequentially as expected [13]. Fibrin matrix is thought to involve in the inflammatory response by

* Corresponding author. School of Basic Medical Sciences / School of Biology & Engineering, Guizhou Medical University, Guiyang, 550025, PR China.

** Corresponding author.

*** Corresponding author.

E-mail addresses: zhoushi@gmc.edu.cn (S. Zhou), longjinhua@gmc.edu.cn (J. Long), zengzhu@gmc.edu.cn (Z. Zeng).

¹ Equal contributing authors.

providing a scaffold for immune cells, such as macrophages and mast cells as well as fibroblast during injury repair process [2,14]. The recruited immune cells contribute to resolve the local inflammation, and fibroblasts contribute to the local tissue reconstruction by secreting collagen, fibronectin, and other extracellular matrix components [15]. Following resolution of the acute inflammatory responses, fibrin eventually replaced by granulation tissues to form new tissue [14].

Fibrin network is a viscoelastic polymer exhibiting both elastic and viscous properties. The elastic component is usually higher than the viscous component, although the viscous component increases rapidly at high rates of deformation [16,17]. Particularly, the elastic component of fibrin matrix usually does not change at lower loads during the rheological experiments, implying that fibrin is a “self-repairing” structure [17]. Fibrin is a highly extensible polymer, which means that under stress blood clots will tend to stretch rather than break [18]. In addition, the non-linear elasticity of fibrin in the form of strain-stiffening and negative normal stress has been observed also in response to deformations [19]. The mechanical properties of fibrin networks depend strongly on their structure and composition determined by the concentration of fibrinogen, thrombin activity and the presence of cells [6]. Numerous studies have denoted that fibrin could regulate the behavior of immune cells which were recruited in Refs. [12,20–22]. Fibrin deposition is a hallmark of mast cell activation [20,21], and the activated mast cells further prompted the accumulation of fibrin around implants by amplifying local inflammation [12]. In contrast to the pro-inflammatory effects of fibrin on mast cells, fibrin matrix exerts a protective effect on macrophages, by preventing inflammatory activation *via* stimuli including LPS and IFN- γ [22].

From viewpoint of immunology, the insoluble fibrin matrix performs important immune regulatory functions which are distinct from the fibrinogen in multiple inflammatory diseases [22]. For example, mice expressing a mutant form of fibrinogen that cannot support fibrin formation exhibit compromised antimicrobial host defense [23]. Macrophages exhibited anti-inflammatory behaviors on fibrin matrix but pro-inflammatory behaviors on fibrinogen [22]. From viewpoint of mechano-biology, the fibrin matrix is a fibrous-like 3D network with unique mechanical properties which can provide wide variety of mechanical stimuli, such as rigidity, topology, adhesion and dimensions for cells [24], and cells must sense these mechanical aspects of their environment and respond appropriately over time for proper cell function [25]. Immune cells have been demonstrated to actively probe and respond to the surrounding physical microenvironments of extracellular matrix (ECM) [26,27], the mechanical sensing and responding machinery of cells are flexibly switched and adapted to work in different dimensions. For example, DCs and neutrophils adopt different migration strategies in 2D and 3D extracellular microenvironments [28]. Thus, the mechanical responses of infiltrating cells to the provisional matrix fibrin appear to be critical for the follow-up immune response and the subsequent wound healing process after biomaterial implantation.

Among the leukocytes present during immune response and subsequent tissue healing after implantation, DCs are considered as master regulators, since they are involved in both the priming and amplification of the innate and adaptive immune responses [29,30]. As antigen-presenting cells, DCs infiltrated in the implantation sites, which generate a battery of adaptive immune responses [29,31]. The potential immunological behaviors of DCs could be critical for the therapeutic effects of these implants and can impact the overall inflammation and tissue repair process [32,33]. Thus, figuring out the exact immune behavior of DCs after implantation and their responses to the provisional matrix fibrin appears to be critical for the rational design of biomaterials.

In the present study, from viewpoint of mechano-biology and immunology (mechano-immunology), an implantation model was developed to elaborate the fibrin formation and immune cells recruitment *in vivo*. An *in vitro* model (100 Pa) using non-toxic and low immunogenic salmon fibrin was constructed to elaborate the DCs physiological behaviors. DCs actively responded to the dimensions of fibrin matrix by

altering morphology and cytoskeleton distribution. Respective changes of mechanophenotypes and immunophenotypes and related intracellular signaling pathways were also discussed.

2. Material and methods

2.1. Reagents and antibodies

Recombinant human granulocyte-macrophage colony stimulating factor (rhGM-CSF), interferon- γ (IFN- γ) and recombinant human interleukin-4 (rhIL-4) were from Peprotech (Rocky Hill, NJ, USA). Dulbecco's phosphate-buffered saline (DPBS) and RPMI medium modified with glutamax were from GE Healthcare Life Sciences (Logan, UT, USA). Lipopolysaccharide (LPS), hematoxylin and eosin (H&E) staining solution, collagenase, dispase II, 4',6-diamidino-2-phenylindole (DAPI), 1,6-diphenyl-1,3,5-hexatriene (DPH), bull serum albumin (BSA) and FITC-conjugated dextran (molecular weight 43 kDa) were from Sigma-Aldrich (St. Louis, MO, USA). Fetal bovine serum (FBS), trizol reagents and revertaid first strand cDNA synthesis kits, and carboxyfluorescein diacetate succinimidyl ester (CFSE) were from Thermo Fisher Scientific (Waltham, MA, USA). Rhodamine phalloidin was from Abcam (Cambridge, MA, USA). Salmon fibrinogen solid and thrombin were from Sea Run Holdings (Freeport, Maine, USA). Cell counting kit 8 (CCK8) was from Dojindo (Rockville, MD, USA). Human interleukin-12 (IL-12) enzyme-linked immunosorbent assay (ELISA) kits and human interleukin-18 (IL-18) ELISA kits were from NeoBioscience (Beijing, China). CD14⁺ magnetic beads were from Miltenyi Biotec (bergisch gladbach, Germany). FITC-conjugated Annexin V and PI (propidium iodide) apoptosis kit was from BioLegend (San Diego, CA, USA).

PE-conjugated anti-human CD11c (clone Bu15), FITC-conjugated anti-human CD80 (clone 2D10), FITC-conjugated anti-human CD86 (clone BU63), FITC-conjugated anti-human CD205 (clone HD30), FITC-conjugated anti-human CCR7 (clone G043H7), FITC-conjugated anti-human HLA-DR (clone L143), FITC-conjugated anti-human CD40 (clone 5C3) antibodies (Abs), APC-conjugated anti-rat OX62 (clone OX-62), FITC-conjugated anti-rat CD45 (clone OX-1) and the corresponding isotype-matched FITC-conjugated anti-human IgG2a (clone MOPC-173), PE, APC and FITC-conjugated anti-human IgG1 (clone MOPC-21) Abs were from BioLegend (San Diego, CA, USA). Rabbit monoclonal Ab against human RhoA (clone EPR18134) or against human CDC42 (clone EPR15620), rabbit monoclonal Abs against rat fibrin (clone EPR2919) and Alexa Fluor 647- or FITC-conjugated goat polyclonal Abs against rabbit IgG were from Abcam (Cambridge, MA, USA).

2.2. Animal experiments and histological staining

The animal experiments were performed with male Sprague Dawley rats (8 weeks, 200–230 g) and were handled in accordance with the requirements of the guidelines for animal experiments, which were approved by the Animal Ethics Committee of Guizhou Medical University. The surgeries were administered under aseptic conditions. Following anesthesia with chloral hydrate (3.5%, w/v, 1 mL/kg), a bone plate (stainless steel 316L) was implanted into the tissue near the tibia. After irrigating wound site with gentamicin saline, the incision was closed with a suture. Medical X-rays (BGL3000, Baiteng Medical, China) were used to detect the position of the bone plates.

The rats were sacrificed 24 h, 48 h and 72 h post-surgery, respectively. The tissues around the bone plates were harvested to assess the DCs recruitment. Tissues were cut into pieces and submerged in medium containing collagenase-1 (200 U/ml) for 15 min, the undigested portions were further ground by porcelain mortar. Leukocytes were isolated from tissue cell suspensions using density gradient media Histopaque-11191 and Histopaque-10771, and centrifuged at 700 g for 30 min. The leukocytes-enriched layer was collected and washed by DPBS with 1% (w/v) BSA at 300 g for 10 min. Isolated leukocytes were suspended in ice-cold DPBS and labeled by APC-OX62 and FITC-CD54 at 10 μ g/mL in

DPBS buffer on ice for 20 min when isotype-matched Abs (FITC or APC-IgG1 antibodies, clone MOPC-21) served as control. After washing in DPBS, the cells were re-suspended in 400 μ L DPBS and analyzed by FACS Calibur cytometer (BD Biosciences, NJ, USA).

The tissues around the bone plates were harvested at 48 h to assess the deposited fibrin matrix and DCs. After being fixed by 4% paraformaldehyde, the tissue samples were processed into tissue sections with a thickness of 6 μ m. For immunological staining, tissue sections were treated with xylene and ethyl alcohol, and were boiled in 10 mM citrate (pH = 6.0) for 90 s, and then were blocked by 5% (v/v) BSA for nonspecific absorption. Then, the sections were incubated with rabbit monoclonal Ab against rat fibrin overnight at 4 °C and FITC-conjugated goat polyclonal Ab against rabbit IgG at 37 °C for 60 min. DCs were labeled by APC-OX62 at 37 °C for 60 min. Nuclei were stained by DAPI (Sigma, USA). For histological staining, the sections were stained with H&E to analyze the tissue morphology. The slides were scanned using a fluorescent microscopy (Nikon, Japan) and confocal laser scanning microscopy (LSM880 NLO, Zeiss, Oberkochen, Germany).

2.3. Rheology measurements

The viscoelastic shear moduli of fibrin matrix were measured using a strain-controlled rheometer (Ares G2 TA rheometer, New Castle, DE USA) with a parallel-plate made of stainless steel with a diameter of 25 mm. To measure the dynamic shear modulus (G') of fibrin, 300 μ L of fibrin were prepared in 24 well plate at 37 °C and transferred immediately onto the plate with temperature holding device. The frequency for the strain sweep test was set at a fixed frequency 1.0 Hz according to literature [19]. All the measurements were performed in a strain-controlled mode at 37 °C, and the edges of the fibrin matrix between the two plates were covered with buffer to prevent the evaporation of water from the samples.

2.4. Isolation and culture of DCs

DCs were generated from human peripheral blood monocytes as described previously [34–37]. Whole human blood was obtained from healthy, unmedicated donors, after informed consent, as approved by the Animal and Medicine Ethical Committee of Guizhou Medical University and conformed to the standards set by the Declaration of Helsinki. Donors were randomized irrespective of sex and age. Briefly, CD14⁺ monocytes from human peripheral blood were isolated by cocktail immune-magnetic beads (Miltenyi Biotec), and the collected cells were suspended in DCs culture media (RPMI 1640, 10% FBS, penicillin/streptomycin, GlutaMax, 800 U/mL rhGM-CSF and 500 U/mL rhIL-4) at a concentration of 10⁶ cells/mL. The purity of DCs were verified using CD11c⁺ biomarker by flow cytometry on day 6. The mDCs were obtained by incubating imDCs with 1000 U/ μ L IFN- γ and 1000 ng/mL LPS for another 2 days.

2.5. Preparation of 2D and 3D culture conditions

The fibrinogen solution was prepared by dissolving salmon fibrinogen solid in Tris buffer (pH = 7.4, 50 mM Tris, 150 mM NaCl) to a concentration of 2 mg/mL, and the fibrin matrix were prepared in 24 well plate at 37 °C. To prepare 2D condition, 125 μ L fibrinogen solution and 125 μ L medium were mixed, and the mix solution with a total volume of 250 μ L was polymerized to fibrin matrix by 5 μ L thrombin (0.1 U/ μ L) at 37 °C for 15 min. The obtained fibrin matrix was cylinder shaped with 2 cm² basal area, and approximately 1 mm thickness. Fibrin matrix was washed three times with medium, and then, 125 μ L cells suspension with a concentration of 1.0 \times 10⁶ cells/mL and another 1 mL medium was added on the top of the fibrin matrix. To prepare 3D condition, cells were immersed in the fibrin matrix. 125 μ L fibrinogen solution and 125 μ L cells suspension were mixed, and polymerized immediately by 5 μ L thrombin (0.1 U/ μ L) at 37 °C for 15 min, the obtained fibrin matrix was cylinder shaped with

2 cm² basal area, and approximately 1 mm thickness, and the fibrin matrix was washed three times. 1250 μ L medium were then added on the top of the fibrin matrix. Thus, 2D and 3D fibrin matrix with same volume and thickness were constructed, and the matrix were immersed in totally 1250 μ L medium as described above, resulting in the same cell concentration in 2D and 3D conditions. The dissolving reagent for fibrin matrix was a solution mixture of Collagenase and Dispase II, which were diluted by DPBS at the final concentration of 0.08% and 0.4% (w/v), respectively.

2.6. Cell microscopy and image analysis

The morphology and actin cytoskeleton of DCs cultured under different conditions were observed and analyzed using scanning electron microscopy (SEM, SU8010, Hitachi, Japan) and confocal laser scanning microscopy (LSM880, Zeiss, Oberkochen, Germany) with a 63 \times /0.95NA objective. For SEM observations, DCs were fixed in 2.5% glutaraldehyde and dehydrated with graded ethanol. Critical point drying was performed using carbon dioxide. After coating with gold, the samples were examined with an SEM. For confocal observations, DCs were fixed in 3.7% formaldehyde solution for 20 min and permeabilized with 0.1% Triton X-100 for 5 min at room temperature. After washing twice with DPBS, DCs were stained with rhodamine-phalloidin (165 μ M) for intracellular actin and 5 μ g/mL DAPI for nuclei. To label intracellular RhoA and CDC42, the cells were incubated, respectively, with rabbit monoclonal Abs against human RhoA or against human CDC42 at 4 °C overnight, and Alexa Fluor 647- or FITC-conjugated goat polyclonal Abs against rabbit IgG at 37 °C for 30 min. The obtained images were analyzed and three-dimensionally reconstructed using Zeiss software.

2.7. Biomechanical characteristics measurements

Young's modulus of DCs were measured by atomic force microscope (AFM, BioScope Catalyst, Bruker, Billerica, MA, USA). Tests were performed in contact mode, and 100 cells were measured for each group. The pyramid probe attached to the cantilever tip was employed to contact a single cell. The spring constant of the cantilever was 0.02 N/m. The Young's modulus of DCs were determined by the force versus distance curves according to the Hertz model [24].

Mobility of membrane lipid molecules of DCs were measured by fluorescence polarization of DPH [34,38]. Briefly, DCs (2 \times 10⁶ cells/mL) were incubated in DPBS containing DPH for 30 min at room temperature. The final concentration of the solvent tetrahydrofuran in which DPH had been pre-dissolved was 0.05%. After centrifugation, DCs were re-suspended in DPBS. Steady-state fluorescence intensity was measured with fluorescence spectrometer (Hitachi, Japan).

Osmotic fragility was measured by treating DCs in isotonic solution (295 mOsm/kg) and hypotonic solutions (55 mOsm/kg and 175 mOsm/kg). After treating with different osmotic buffers for 30 min, the numbers of non-hemolytic DCs were counted using cytometer (Millipore, USA).

2.8. Flow cytometry analysis

Flow cytometry was performed using a FACS Calibur cytometer (BD Biosciences, NJ, USA). For immune-phenotypes analysis, human DCs were incubated with anti-CD80, -CD86, -CD40, -CD11c, -CCR7, -HLA-DR, or -CD205 Abs at 10 μ g/mL in DPBS buffer on ice for 20 min, isotype-matched Abs served as control. After washing in DPBS, the cells were re-suspended in DPBS and analyzed by flow cytometry.

The apoptosis of DCs was quantified by FITC-conjugated Annexin V and PI apoptosis kit. DCs were incubated with FITC-conjugated Annexin V in DPBS buffer on ice for 20 min, and PI on ice for 5 min. After washing by DPBS, the cells were re-suspended in DPBS and analyzed by flow cytometry. Cells stained with FITC-conjugated Annexin V denoted the early stage apoptosis and the cells stained with both FITC-conjugated Annexin V and PI denoted the late stage apoptosis.

Endocytic activities of imDCs were determined by FITC-conjugated dextran, as described previously [39]. Briefly, pre-warmed FITC-conjugated dextran solution was mixed with the cell suspension (the final concentration of FITC-dextran in the medium was 500 $\mu\text{g}/\text{mL}$). After incubating at 37 $^{\circ}\text{C}$ for 2 h, the cells were washed 3 times with DPBS containing 2% FBS to remove particles that had not been endocytosed. Co-culture of imDCs with FITC-dextran on ice was used as a blank control group (non-specific adsorption). The percentage of imDCs showing endocytosis was analyzed using flow cytometry.

2.9. Mixed leukocyte reaction and ELISA assay

Human allogeneic T cells (1×10^6 cells/mL) were used as the responder cells, and their proliferation analysis was based on the intracellular fluorescent dye CFSE. The mixed leukocyte reaction (MLR) assays were performed in 96-well plates (Corning, USA) by co-culturing CFSE labeled T lymphocytes and mDCs in terms of the mDCs and T cell concentration ratios of 1: 1. After incubating for 3 days, Cells were then harvested and analyzed using flow cytometry.

The expression levels of interleukin-12 (IL-12) and interleukin-18 (IL-

18) in culture supernatant were quantified using ELISA kits. Briefly, the supernatant was collected and then centrifuged at 1000 rpm for 5 min. Supernatant or standard sample (100 μL) was added into a 96-well plate pre-coated with anti-human IL-12 or IL-18 primary antibodies. The plate was examined at 450 nm using the iMark™ microplate reader (BIO-RAD, Hercules, CA, USA). A four-parameter standard curve was obtained using the absorbance ratio of the yellow product to the value of the standard sample, as per the manufacturer's instructions.

2.10. Quantitative real-time reverse transcription-PCR (qRT-PCR)

Cultured cells were collected at the endpoint of each phase. Total RNA from DCs was extracted using Trizol. First-strand cDNA samples, as the templates for qRT-PCR, were reverse-transcribed using a RevertAid First Strand cDNA Synthesis Kit. QRT-PCR analyses were performed using a quantitative real-time amplification system (QuantStudio 7, Thermo Fisher) with primers specific for extracellular regulated protein kinases (ERK), CDC42 and RhoA. Glyceraldehyde-3-phosphate dehydrogenase (GAPDH) was used as an internal control to normalize mRNA expression levels. The primers sequences are listed in [Supplementary](#)

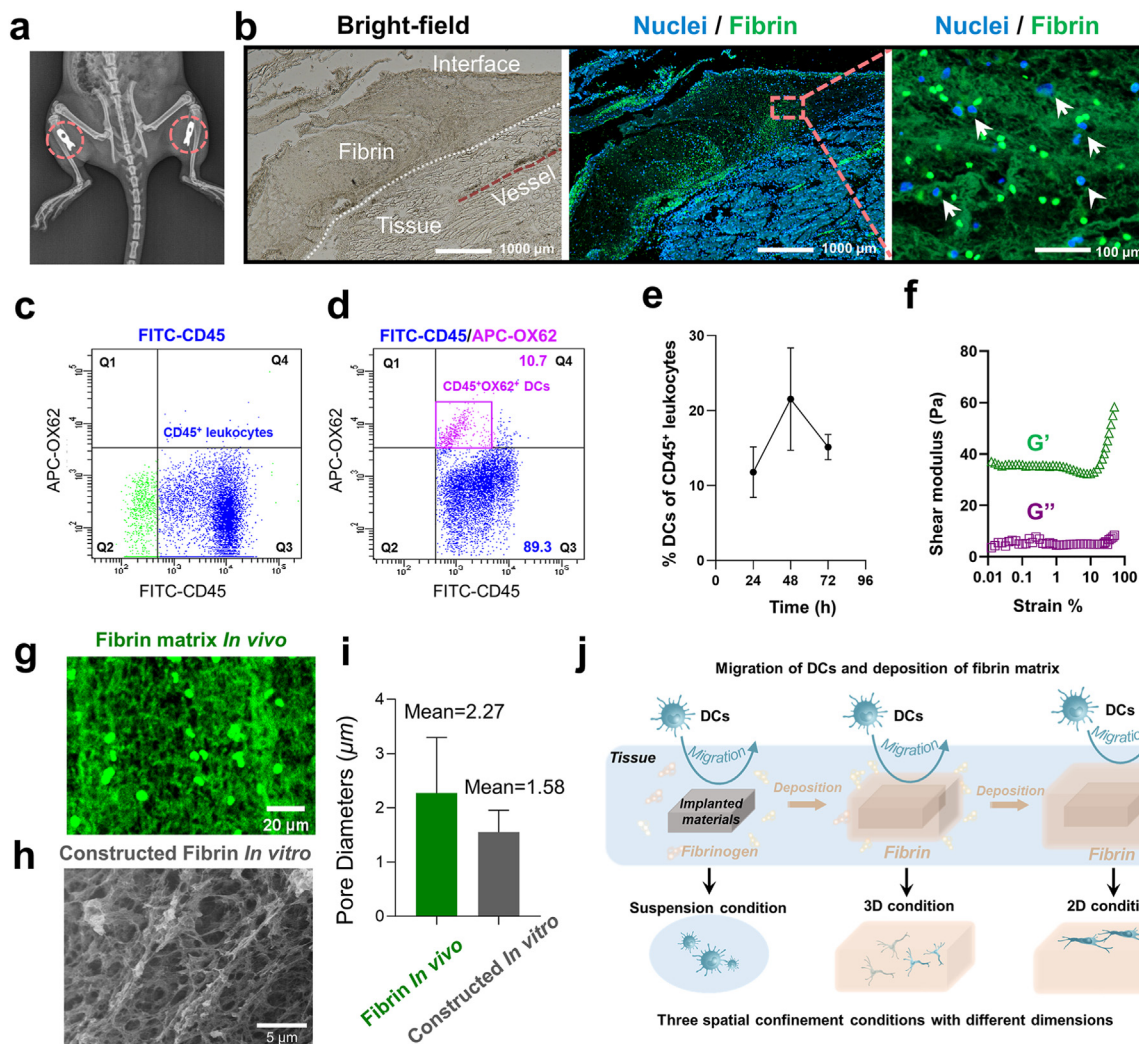


Fig. 1. Fibrin matrix deposition and DCs recruitment after implantation. (a) The medical X-rays image of bone plates implanted into tissue near the tibiae of the rat. (b) Immunofluorescent staining for *in vivo* deposited fibrin matrix: bright-field image, fluorescence staining of nuclei (blue) and fibrin (green), high-magnification image of fibrin matrix (respectively, from left to right). (c) Flow cytometry analysis for rat leukocytes of implantations sites. Cells were labeled by FITC-CD45. (d) Representative scatter image of the OX62⁺ CD45⁺ DCs groups in CD45⁺ leukocytes. (e) The ratios of DCs to leukocytes at 24 h, 48 h, 72 h post-implantation. (f) Rheological behavior of fibrin matrix. (g) Immunofluorescent image of fibrin matrix *in vivo*, scale bar, 20 μm . (h) SEM image of fibrin matrix constructed *in vitro*, scale bar, 5 μm . (i) Statistical analysis for pore diameters of fibrin matrix *in vivo* and constructed *in vitro*. (j) Schematic diagram of the three conditions for DCs during the fibrin matrix deposition. $n = 3$ biologically independent measurements, mean \pm SD, * $p < 0.05$, ** $p < 0.01$.

Table 1. The $2^{-\Delta\Delta CT}$ method was used to calculate the fold-change, CT denotes the cycle number when the fluorescence signal of the amplification plot passed the fixed threshold.

2.11. Statistical analysis

All data are presented as the mean \pm standard deviation (SD). A Student's *t*-test or Mann-Whitney test was performed, depending on whether the data pass the normality test for two-group comparison. One-way ANOVA test followed by Newman-Keuls test was used for multiple-group comparison, while non-parametric Kruskal-Wallis test followed by Dunn's test was applied when the data cannot pass the normality test. All statistical analyses were performed using Prism statistical software (GraphPad Software, CA, USA). **p* < 0.05; ***p* < 0.01; ****p* < 0.005.

3. Results

3.1. DCs were recruited to the pathophysiological and mechanical microenvironment of fibrin matrix after implantation

To confirm fibrin matrix formed around the implants, we implanted commercial bone plates into tissue near the tibiae of rats (Fig. 1a and Supplementary Fig. 1a-f) and harvested the tissues around the bone plates at 48 h after implantation. The immunofluorescence (Fig. 1b) and immunohistochemistry images (Supplementary Figure 1g) showed that a large amount of fibrin matrix deposited on the interface between the tissue and bone plates. This deposited fibrin matrix presented a fibrous-like network (Supplementary Figure 1h), and numerous nucleated cells (blue, white arrows in Fig. 1b) infiltrated into the fibrin matrix and were netted in this network. To confirm the presence of DCs in these nucleated cells, DCs of rats were detected by APC-OX62 antibody according to the literature [40]. The results indicated that DCs (red) recruited to the site of fibrin matrix after implantation (Supplementary Figure 1h). Furthermore, in order to confirm above observations and to figure out the recruitment kinetics of DCs, leukocytes around the implanted sites are collected at 24 h, 48 h and 72 h post-implantation, respectively and analyzed using flow cytometry (Fig. 1c and d, Supplementary Figure 2). The whole leukocytes were labeled by FITC-CD45 [41], where DCs can be recognized by APC-OX62 at the same time (Fig. 1d, Supplementary Figure 2). The ratios of DCs to leukocytes reached the highest at 48 h (Fig. 1e) [42]. Taking together, as shown in Fig. 1b–e, DCs were recruited to the fibrin matrix after implantation, the time window between fibrin deposition [2] and DCs massive recruitment overlaps.

To further characterize the micro-structure of the fibrin matrix and investigate the response of DCs, we prepared fibrin matrix *in vitro* to mimic the deposited fibrin matrix (1 mg/mL fibrinogen, according to the physiological concentration [31]). Considering the viscoelasticity property of fibrin matrix, the mechanical property of fibrin matrix prepared *in vitro* was measured by rheological experiments (Fig. 1e). The elastic component (shear storage modulus G') was higher than the viscous component (shear dissipative modulus G''), implying that fibrin matrix behaves like an elastic solid. The G' remained constant first but then began to grow sharply with increasing shear strain. The obtained G' in stabilization stage was about 35 Pa which estimated to 100 Pa in Young's modulus according to formula [43]. The fibrin matrix constructed *in vitro* had a dense fibrous-like network structure as fibrin *in vivo* (Fig. 1g and h), and the pore diameter of fibrin matrix *in vivo* and constructed *in vitro* seems to be similar (Fig. 1i), considering the 30% shrinkage of electron microscopy (SEM) samples [44]. Since the pore diameters of the fibrin matrix were much smaller than the typical size of human DCs (Fig. 1h), thus, from viewpoint of mechanobiology, it was reasonably speculated that DCs experience three mechanical environments (Fig. 1j): (I) DCs are exposed in the tissue fluid (suspension conditions) without fibrin and mechanical supports; (II) DCs migrate to target locations and infiltrate into the fibrin matrix (3D conditions); (III) DCs arrive at target locations and adhere on the surface of the fibrin matrix (2D conditions).

3.2. DCs exhibited featured morphologies in fibrin matrix

As the pathophysiological and mechanical alteration of extracellular environments are key to DCs immunological behaviors at the site of implantation, here, the morphology of DCs cultured in different conditions as Fig. 1j described were characterized (Fig. 2). Both imDCs and mDCs were induced according to our previous methods, and the expression of phenotypic molecules (summarized in Supplementary Fig. 3) confirmed that both imDCs and mDCs were successfully obtained. The imDCs and mDCs cultured on the surface of fibrin matrix to mimic 2D conditions (imDCs-2D and mDCs-2D), and inside of fibrin matrix to mimic 3D conditions (imDCs-3D and mDCs-3D). In parallel, imDCs and mDCs cultured in medium to mimic normal suspension conditions were labeled as imDCs-S and mDCs-S. As the images, DCs presented a featured morphology with polarized cell body and elongated dendrites in or on fibrin matrix, and the deformation processes of DCs were dynamic and gradual, and reached relatively stable state at 6 h (Supplementary Fig. 4). SEM imaging further confirmed the featured ultra-structures of DCs at 6 h (Fig. 2a and b). The imDCs-S and mDCs-S exhibited a polygonal shape with large membrane ruffles and filopodia as reported previously [45]. DCs spread and elongated on fibrin matrix (imDCs-2D and mDCs-2D) and were completely wrapped by the fibrin matrix (imDCs-3D and mDCs-3D) with micro-spikes shuttled through the mesh gaps in the fibrous-like network (Supplementary Fig. 5).

As cytoskeleton of DCs are key in initiating cell deformation [46–48], further examination of their distribution on DCs indicated that DCs responded to the network of fibrin matrix through F-actin reorganization, and DCs addressed the different mechanical environments in different ways (Fig. 2c and d). For imDCs-S and mDCs-S, F-actin mainly located at the circular edge of the cell bodies and away from the nuclei; imDCs-2D and mDCs-2D elongated, leading to a predominantly bi-polarized shapes; In 3D conditions, both DCs stretched in several directions resulting in a predominantly tri-polarized or stellate spindle-shaped morphology. Taking together, the observations from Fig. 2, these results suggested that the featured morphology and reorganized F-actin likely results from the distinct response mode of DCs to mechanical environments derived from fibrin matrix.

3.3. DCs depolarized rapidly but got altered mechanophenotypes

In order to elucidate that the altered morphology of DCs was due to the fibrin matrix derived mechanical factors, the fibrin matrix was dissolved and the dynamics of cells deformation were observed. During the dissolution process (Supplementary Fig. 6a-d), DCs remodeled rapidly and gradually depolarized. These results suggested that morphologies of DCs were high dynamic, and relied on the mechanical environments. The apoptosis analysis of cells which harvested from fibrin matrix (Supplementary Fig. 7) denoted no apoptosis, meanwhile, the F-actin contents of DCs from fibrin matrix were detected but there were also no significant differences compared with intact DCs which sustained in suspension (Supplementary Fig. 6e and f). In contrast, the viabilities of DCs harvested from fibrin matrix were enhanced (Supplementary Fig. 8), which suggested that DCs actively perceived the external environment and made appropriate internal configuration adjustments spontaneously.

In order to further characterize and elucidate the intrinsic features of DCs harvested from fibrin matrix, the mechanophenotypes including young's modulus, mobility of membrane and osmotic fragility were used to evaluate the potential changes of DCs (Fig. 3). After experiencing fibrin mechanical microenvironments, the young's modulus of imDCs (Fig. 3a–d) were increased, which indicated the increased stiffness of imDCs. Polarization values of imDCs dramatically increased (Fig. 3i), indicating that the mobility of membrane lipid molecules of imDCs decreased. The increased stiffness (Fig. 3a–d), reduced membrane microfluidity (Fig. 3i) and the enhanced strength (Fig. 3k) could raise the difficulties of membrane distortion of imDCs. For mDCs, after experiencing mechanical environment of fibrin, the reduced stiffness

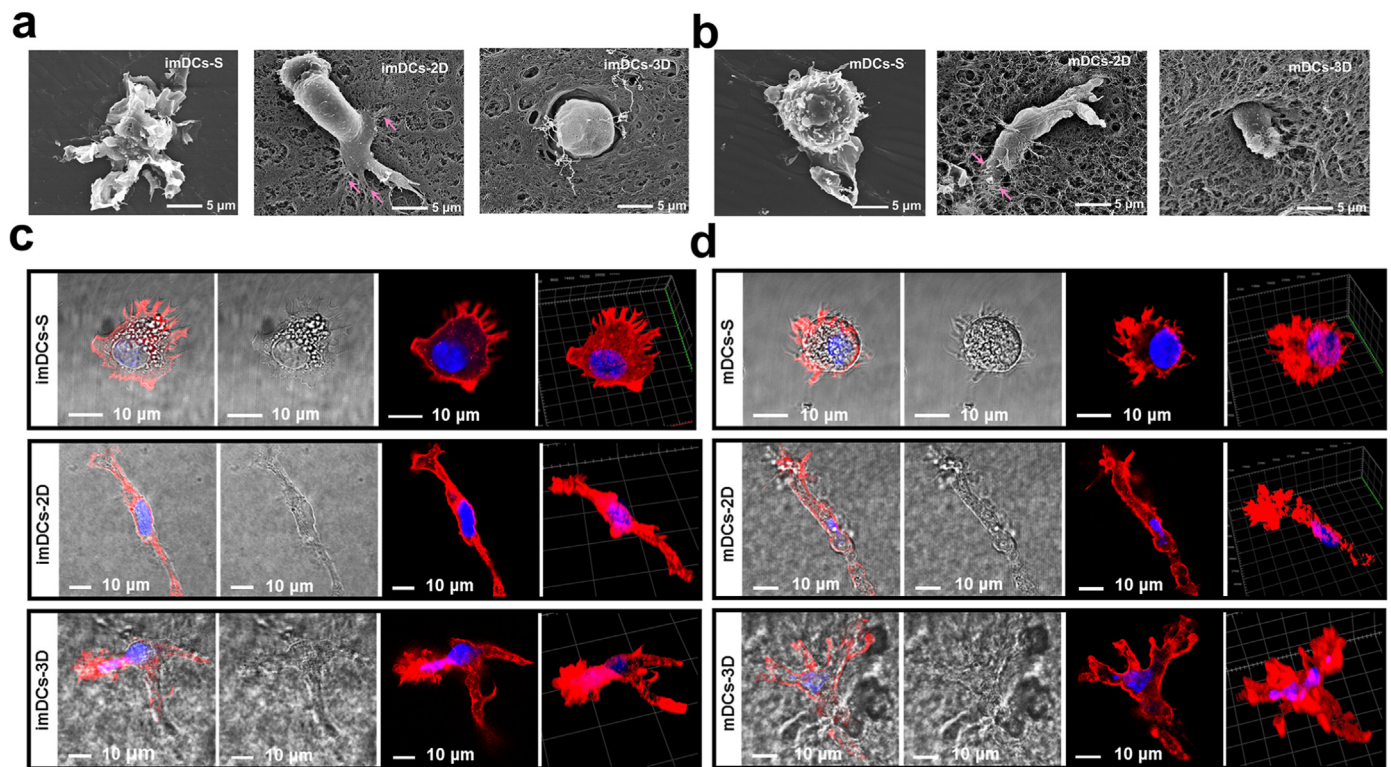


Fig. 2. DCs exhibited featured morphologies in fibrin matrix. (a, b) Representative SEM images of imDCs (a) and mDCs (b) cultured by fibrin matrix at 6 h. (c, d) Representative confocal images of cytoskeleton of imDCs (c) and mDCs (d) cultured in different conditions at 6 h. From left to right are merged images, bright-field images, fluorescence images of F-actin (red) and nuclei (blue), 3D reconstruction of fluorescence images, respectively.

(Fig. 3e–h) and of enhanced membrane strength (Fig. 3j) suggested mDCs became softer. These results above indicated that DCs were reshaped and obtained altered mechanophenotypes in responding to mechanical dimensions of fibrin matrix.

3.4. Fibrin matrix with mechanical dimensions directed DCs immunophenotypes

Next, the immunophenotypes of DCs were further explored. DCs serve two main functions in their lifespan, including antigen sampling of imDCs, and presenting antigen to T lymphocytes by mDCs. During the maturation process of imDCs differentiate into mDCs, the surface molecules of imDCs including CD80, CD86 and HLA-DR (human leukocyte antigen-DR) were increased (Fig. 4a, Supplementary Fig. 3a–f) [36,49]. Thus, in order to elucidate the DCs immunological responses, the immunophenotypes of DCs including function-associated molecules and immune functions were examined. Function-associated molecules of imDCs including CD80, CD86 and HLA-DR were characterized by flow cytometry. The expression levels of CD80 (Fig. 4b) and HLA-DR (Fig. 4d) of imDCs remained unchanged, and the expression levels of CD86 (Fig. 4c) slightly upregulated in 2D condition. Taking note of the fact that the expression levels of CD86, CD80 and HLA-DR in each imDCs group were markedly lower than those of mDCs-S, which indicated that the fibrin matrix did not induce imDCs maturation. The endocytic capabilities of imDCs were analyzed using FITC–dextran to mimic antigens. DCs were harvested from 2D and 3D fibrin matrix after culturing for 3 h, 6 h and 48 h, respectively. In line with the results of CD205 (an endocytic receptor on the membrane surface of imDCs [50]) (Fig. 4e), the endocytic capabilities of both imDCs-2D and imDCs-3D were dramatically declined (Fig. 4f).

The key immune function of mDCs is to activate naïve T cells, which in turn cause the initiation of adaptive immune response [49]. The naïve T cells priming process requires a multi-signal reactivity between mDCs

and T cells. Signal 1 of specific antigens peptide in the context of MHC molecules (HLA-DR molecules for human) on the cell surface, signal 2 of costimulatory molecules including CD80 and CD86 upregulation, signal 3 of interleukin secretion including IL-12 and IL-18 [51,52]. The results above (Fig. 4b–d) indicated that the expression levels of HLA-DR remained unchanged but CD80 and CD86 upregulated, suggesting increasing communications between mDCs and T cells (in the immune synapse) [53]. CFSE experiments were applied to evaluate the functions of mDCs activating naïve T cells (Fig. 4g and h). The results denoted that the mDCs-2D displayed an obvious enhancement of T cells priming capabilities at various ratios of mDCs and T cells, while the mDCs-3D exhibited a relatively small increase. Moreover, noticeable increases in the IL-12 and IL-18 secretion levels for mDCs-2D (Fig. 4i and j), indicated their increased capabilities of priming and activating naïve T cells [54]. These results above indicated that DCs immunophenotypes were directed by fibrin matrix with mechanical dimensions, and imDCs obtained negative effects on the endocytic capabilities, mDCs got positive effects on the capabilities of priming and activating naïve T cells.

Given the fact that the fibrin matrix formation process was initiated by the protease thrombin, to further confirm the effects of thrombin, we also detected the functions and phenotypes of imDCs and mDCs treated by thrombin for 6 h (final concentration of 0.5 U/ml in our system). There were no significant differences between intact groups and thrombin treated groups of imDCs and mDCs on the phenotypes including CD80, CD86, HLA-DR and the immune functions including endocytosis capability of imDCs and T cells priming capability of mDCs (Supplementary Fig. 9).

3.5. RhoA and CDC42 signaling pathways involved in DCs mechano-immunological coupling mechanisms

To elucidate the underlying mechanisms of the immunophenotypes and mechanophenotypes conversions of DCs in responding to the

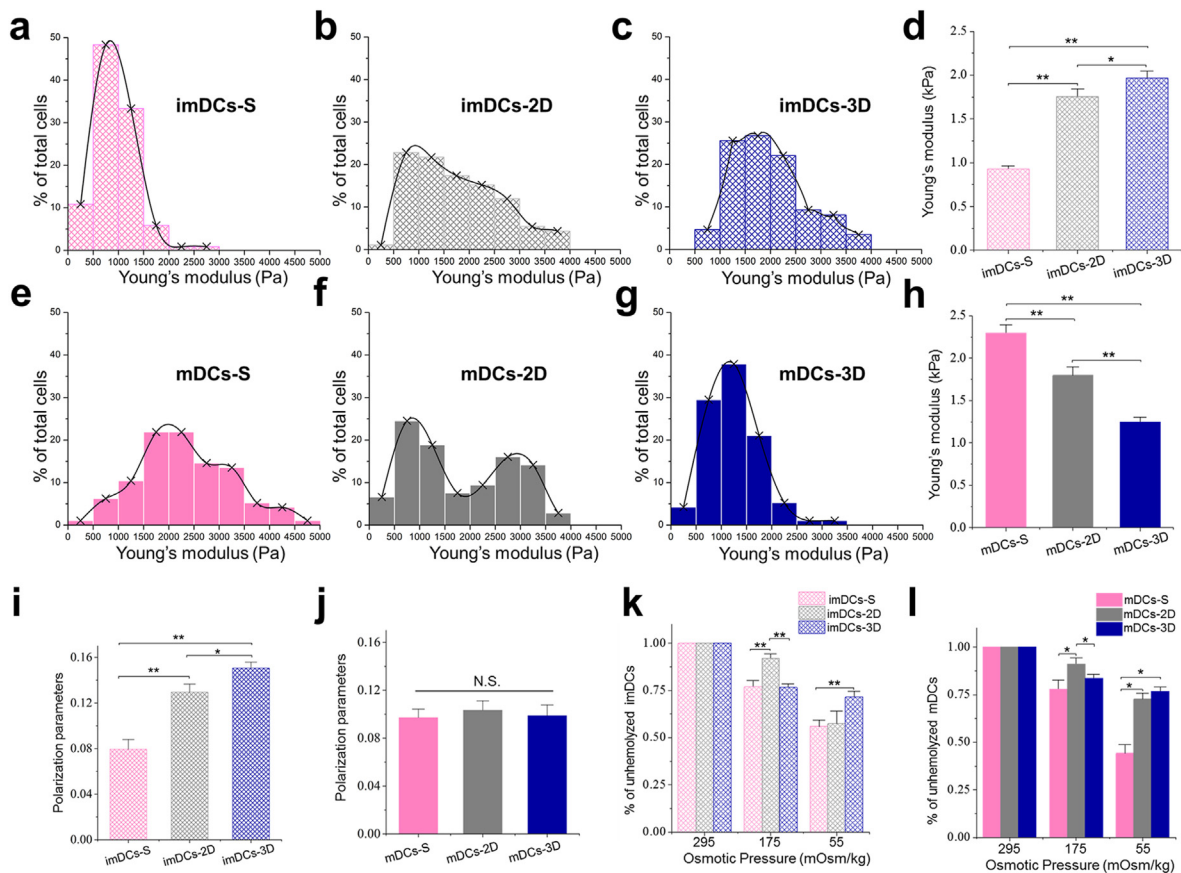


Fig. 3. mechanophenotypes characterization. (a–d) Young's moduli of imDCs. Frequency-distribution histogram (a–c) and the statistical analysis (d) of the Young's modulus values of imDCs. (e–h) Young's moduli of mDCs. Frequency-distribution histogram (e–g) and the statistical analysis (h) of the Young's modulus values of mDCs. (i, j) Fluorescence polarizations of imDCs (i) and mDCs (j). (k, l) Osmotic fragilities of imDCs (k) and mDCs (l). $n = 3$ biologically independent measurements, mean \pm SD, * $p < 0.05$, ** $p < 0.01$.

mechanical microenvironments, the key regulatory molecules of DCs including RhoA and CDC42 were analyzed, as RhoA and CDC42 as two kinds of important Rho GTPase, involved in not only the F-actin structures but also the DCs immune functions [55–57]. Here a tri-color confocal imaging was utilized to elucidate the potential roles of RhoA and CDC42 on DCs (Fig. 5a and b). Results indicated that the distribution of RhoA on DCs was organized to form small punctate clusters and co-localized with nuclei of DCs which obtained from the fibrin matrix, implying the distribution of RhoA was reconstructed (Fig. 5a). Furthermore, the fluorescent intensity of RhoA was significantly decreased for imDCs (Fig. 5c) and were significantly enhanced for mDCs (Fig. 5e). The fluorescent intensity of RhoA in nuclear regions was significantly enhanced as the images (Fig. 5d, f). The expression levels of CDC42 were also up-regulated for both imDCs and mDCs after treating by fibrin matrix derived mechanical microenvironments (Fig. 5b, g, h).

Finally, to further confirm above observations, quantitative PCR was applied to detect these changes. In line with the data from qualitative analysis on RhoA fluorescent intensity of imDCs (Fig. 5c) and mDCs (Fig. 5e), the mRNA expression levels of RhoA of imDCs (Fig. 5i) and mDCs (Fig. 5j) were decreased also after treating by 2D and 3D fibrin matrix. The mRNA expression levels of CDC42 of imDCs (Fig. 5i) and mDCs (Fig. 5j) also increased, which is consistent with the results of fluorescence intensity analysis (Fig. 5g and h), except for the decreasing trend in the imDCs-2D group. Taken together, these results above suggested that in response to 2D and 3D fibrin matrix loading, the actin cytoskeleton undergoes initial rearrangements that influence intracellular Rho GTPase including RhoA and CDC42, which were reported involved in DCs subsequent immune responses [55–57]. In addition, ERK pathway as the upstream of the Rho GTPase signals, which has found to

be required in activation of stress fiber contractility [58,59]. ERK also reported as playing a critical role in chemical and mechanical signals integrating [59]. To further detect the intracellular effector molecules of DCs, the expression levels of ERK were also analyzed. Results indicated that the expression levels of ERK were significantly increased in both imDCs (Fig. 5i) and mDCs (Fig. 5j), implying that ERK acted as potential effector molecules during F-actin reorganization after mechanical stimulation.

4. Discussion

At the implantation site, the changed local immune microenvironments including pathophysiological and mechanical alterations are key to DCs immunological behaviors. According to our immunofluorescence and flow cytometry results (Fig. 1a–e, Supplementary Fig. 1h), DCs recruited to the implantation site soon afterwards, which play a special role in regulating the subsequent wound healing or inflammatory processes [31,33,60]. Here, we demonstrated that DCs have undergone significant deformation and F-actin reorganization at the fibrin matrix sites in the mechanical dependent manner, afterwards, DCs got altered mechanophenotypes, which coupled with their immunophenotypes in the follow-up immune processes. RhoA and CDC42 signaling pathways involved in DCs mechano-immunological coupling mechanisms. This work underlined the importance of the mechanical factors of fibrin matrix in regulating the cells functions, which contributed to improve our understanding of the evaluation of the materials biocompatibility *in vivo*.

DCs, like most migratory immune cells, scattered throughout the body and have the potential to infiltrate any type of tissue with various mechanical properties, including 2D and 3D microenvironments [26–28,

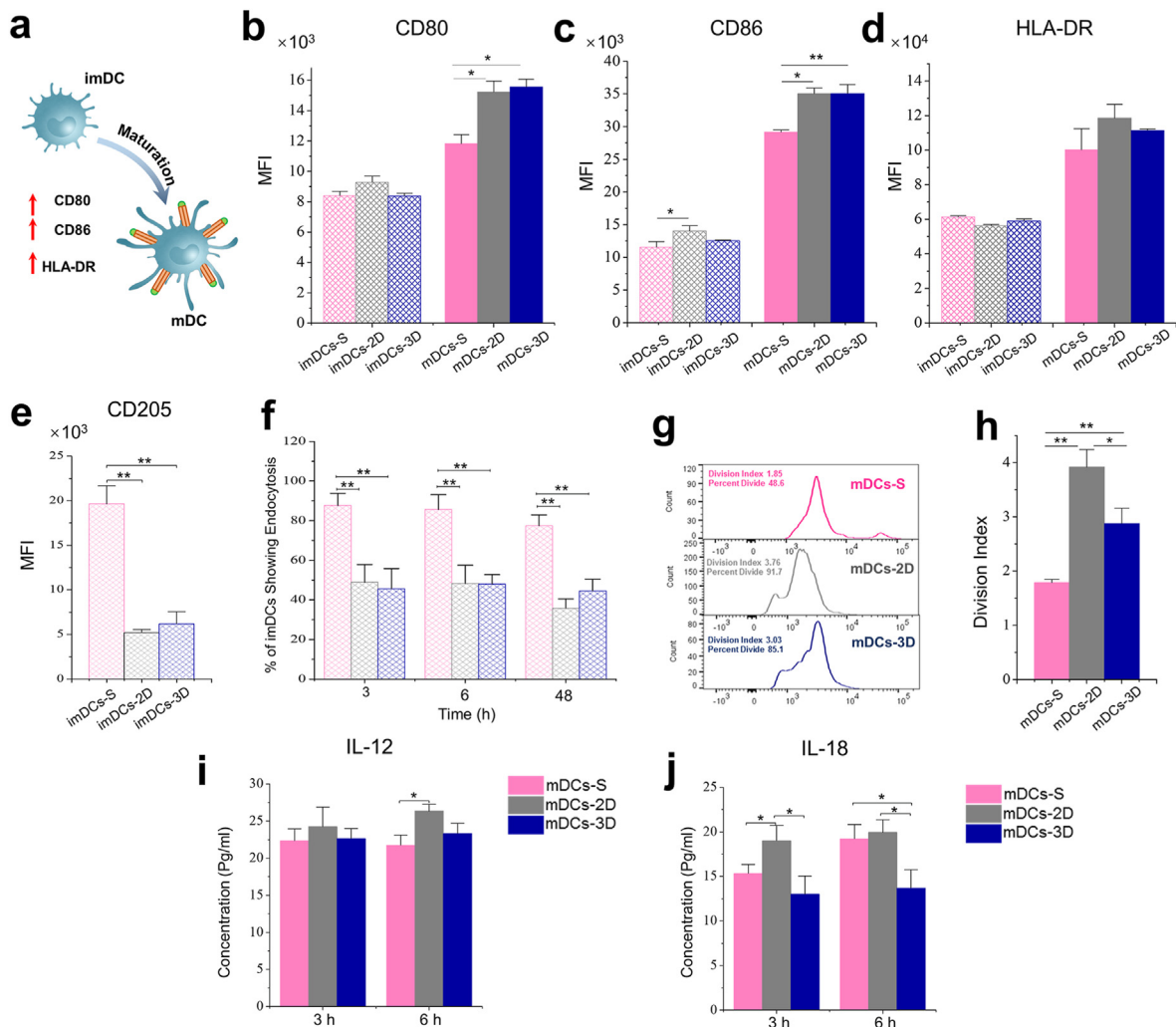


Fig. 4. DCs immunophenotypes analysis. (a) Surface molecules changing of imDCs during maturation process. (b–e) Flow cytometer analyses for functional associated surface molecules of imDCs and mDCs. (b) CD80, (c) CD86, (d) HLA-DR, (e) Flow cytometer analyses for CD205 of imDCs. (f) Endocytosis activities of imDCs. The imDCs were taken out from different conditions after culturing in fibrin for 3 h, 6 h and 48 h, respectively. (g–h) Proliferation of T cells was measured by CFSE dilution at 72 h post-activation mDCs treated by 2D and 3D fibrin matrix for 6 h, mDCs-S served as control. (g) Representative CFSE dilution from a single experiment. (i, j) ELISA analyses for IL-12 (i) and IL-18 (j) of mDCs supernatants at 3 h and 6 h treated by 2D and 3D fibrin matrix. Values represent the mean \pm SD, $n = 3$ biologically independent measurements, * $p < 0.05$, ** $p < 0.01$.

61–64]. It's well known that ECM dimensions have a significant impact on cellular behavior [61,65]. Previously, investigations of DCs within 3D matrices have demonstrated differences in cell chemotaxis behaviors and morphologies when compared with 2D flat surfaces or cells seeded on top of collagen gels [26,28]. Here, basing on the deposited fibrin matrix with fibrous-like network and the recruited DCs which seemingly netted in this network *in vivo*, we proposed that DCs might have experienced different ECM dimensions, and we established *in vitro* models to mimic the ECM microenvironments with 2D and 3D fibrin matrix (Figs. 1g–j). The observed images denoted that DCs exhibited obvious morphological deformation and cytoskeletal remodeling under different dimensional fibrin matrix, and DCs presented featured morphologies and F-actin distribution in 2D and 3D fibrin matrix (Fig. 2). These features suggested that different intracellular contractile force patterns of cells matched diverse local mechanical conditions.

Furthermore, to establish the relationship between the intracellular contractile force and external mechanical conditions, we observed DCs shape reformation in fibrin matrix (Fig. 2, Supplementary Figs. 5) and recovery during fibrin matrix dissolution (Supplementary Fig. 6). Such mechanical-featured cell deformation was in line with previous observations revealed two phenotypically distinct modes of migration and

shape in varied alignment and stiffness of synthetic 3D fiber matrices [66]. Thus, DCs have the ability to actively perceived the external environment and made appropriate adjustments spontaneously in response to the external mechanical stimuli.

Functions of cells *in vivo* are driven by a wide variety of factors mainly related to the extracellular environment, which refers to ECM together with the biomechanical environment [67,68]. Here, DCs obtained distinct mechanophenotypes and immunophenotypes in response to external mechanical conditions (Figs. 3 and 4), we hypothesized that such mechanophenotypes transitions are coupled with their immunophenotypes. The increased stiffness, reduced membrane micro-fluidity and enhanced membrane tension meant poor deformability, which could be contributed to their weakened endocytic capabilities (Figs. 3 and 4), because phagocytosis of imDCs is a dynamically process involving cell deformation and plasma membrane distortion [69,70]. For mDCs, decreased stiffness of mDCs suggested the increased deformability of mDCs which might be alter cellular mechanical characteristics and result to the special mechanophenotypes of DCs. Taken together, these results suggested that the dimensionality of the fibrin matrix (2D and 3D) accounts for a very disparate response of DCs, including the mechanophenotypes and immunophenotypes, thus emphasizing the potential

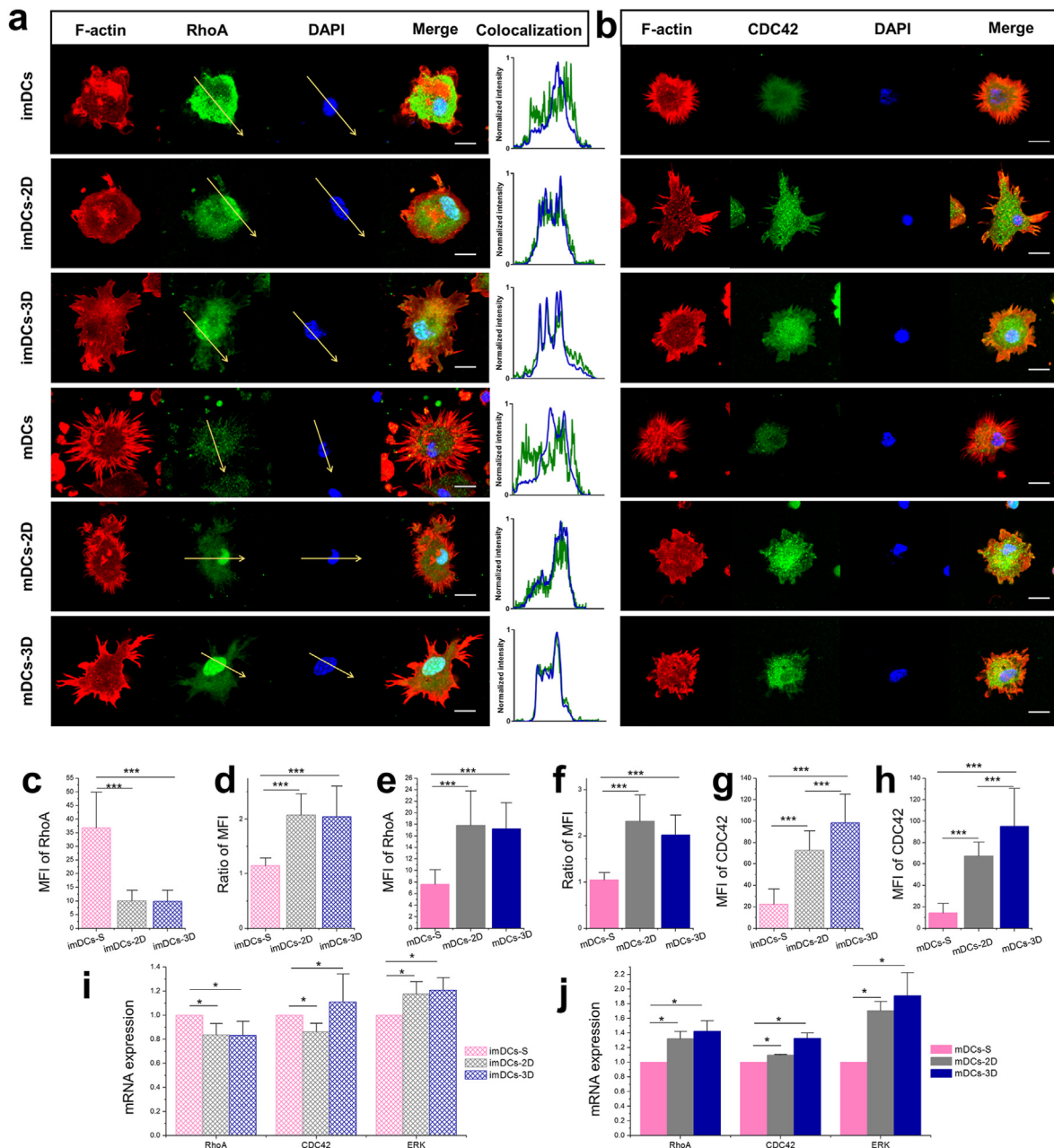


Fig. 5. RhoA and CDC42 signaling pathways involved in DCs mechano-immunological coupling mechanisms. (a) Representative confocal images of cytoskeleton and RhoA of DCs collected from different conditions at 6 h. From left to right are fluorescence images of F-actin (red), RhoA (green), nuclei (blue), merged fluorescence images and corresponding fluorescence intensity profiles across yellow lines, respectively. (b) Representative confocal images of cytoskeleton and CDC42 of DCs collected from different conditions at 6 h. From left to right are fluorescence images of F-actin (red), CDC42 (green), nuclei (blue) and merged fluorescence images, respectively. (c) Mean fluorescence intensity of RhoA of imDCs. (d) The normalized mean fluorescence intensity ratio of imDCs nucleus regions to cell body regions. (e) mean fluorescence intensity of RhoA of mDCs. (f) The normalized mean fluorescence intensity ratio of mDCs nucleus regions to cell body regions. (g, h) mean fluorescence intensity of CDC42 of imDCs (g) and mDCs (h). (i, j) RT-qPCR analysis for mRNA expressions of imDCs (i) and mDCs (j). Values represent the mean \pm SD, $n = 3$ biologically independent measurements, * $p < 0.05$, ** $p < 0.01$.

mechanical reprogramming processes that cell egress through the surrounding matrix.

The results of mechanophenotypes and immunophenotypes revealed that the immunological behaviors of DCs were modulated: negative effects on the endocytic capabilities of imDCs and positive effects on the capabilities of mDCs to activate naïve T cells (Fig. 4). Thus, the overall biological process after implantation could be proposed as following, insensitive imDCs prevent the excessive-immunity and the amplification of inflammatory signals, and activated mDCs contribute to the elimination of existing antigen. As the bridge of innate and adaptive immune

system, DCs may play a positive regulatory role in the early injury repair after implantation. Moreover, our results revealed that the sensitivity of imDCs to dimensions were different from that of mDCs. For instance, the function of mDCs was seemingly susceptible to the dimensions, which manifest as the increased capabilities of activation naïve T cells on 2D fibrin matrix (Fig. 4). It could be speculated that, during the process of DCs differentiation (imDCs into mDCs), mDCs appeared to more sensitive to mechanical environments. It appeared reasonable that imDCs pass through tissues with widely different mechanical microenvironments to search and uptake antigens [48,71,72], and they could be maintaining

impervious to tissues mechanical environment in order to search more efficiently in a labor-saving way.

Cell has specialized machinery for ECM mechano-sensing and mechano-transduction, including motor proteins, cytoskeletal proteins, and force-sensitive proteins in response to forces [46,66,68]. In this study, the key regulatory molecules including RhoA and CDC42 which involved in the regulation of cell morphologies, F-actin structure and cell functions of DCs were analyzed (Fig. 5) [55–57,73]. ERK which has found to be required in activation of stress fiber contractility and integrating chemical and mechanical signals was also detected [58,59]. Previous studies have addressed RhoA acts to drive contraction and detachment of the dendrites, CDC42 serves to promote cellular extension and filopodia formation in DCs [57,73]. Besides the regulation of cytoskeletal organization, antigen capturing, endocytosis, contact formation of DCs with T cells and subsequent T cell activation were also critically regulated by RhoA and CDC42 [55,56,73]. Thus, it is likely that DCs require RhoA/CDC42/ERK signals to reorganize cells mechanophenotypes and immunophenotypes in responding to the microenvironmental mechanical factors. Additional investigations are still required to elucidate the intimate relationships between mechanophenotypes and immunophenotypes in 2D and 3D microenvironments.

Finally, the fibrin hydrogels have been widely used and reported as a sealant or glue [74], a matrix for cells [75], a scaffold for tissue engineering [76], and a carrier and/or a vector for targeted drug delivery [77]. The fibrin hydrogels can be manipulated to enhance or suppress DCs function to promote a specific desirable immune response during implantation, which would improve the therapeutic activity of the implants. Thus, DCs loaded by fibrin can a new possibility for implantable biologically active therapeutics, and may suggest a simple yet potentially powerful approach to modulate DCs immunophenotypes by providing different external mechanical microenvironment. On the other hand, DCs are capable of inducing immune responses or mediating tolerance, both of which are critical to regulating host response to implants and the subsequent wound healing process [29,31,78].

5. Conclusions

Fibrin matrix deposition following biomaterial implantation resulted in changes of local immune and mechanical microenvironments for recruited DCs. DCs were sensitive to mechanical cues of fibrin matrix and exhibit morphological and cytoskeletal deformation under different dimensions. After experiencing fibrin matrix, DCs got altered mechanophenotypes and immunophenotypes which depended on the dimensions of the fibrin matrix and differentiation stages of DCs. F-actin and the RhoA and CDC42 signaling pathways were involved in DCs mechano-immunological coupling mechanisms. Thus, our findings not only emphasize the role of deposited fibrin in modulating the behaviors of DCs but also contribute to a better understanding of the precise process of immune responses triggered by biomaterial implantation.

Data availability statement

The data sets used and/or analyzed during the current study are available from the corresponding author on reasonable request.

Credit author statement

Wenhui Hu: Investigation, Methodology, Formal analysis, Data curation, Writing - original draft. **Yun Wang:** Investigation, Formal analysis, Data curation, Writing - original draft, Funding acquisition. **Jin Chen:** Methodology, Investigation. **Wenhui Hu, Yun Wang and Jin Chen** contributed equally to this work. **Peng Yu:** Investigation. **Fuzhou Tang:** Investigation. **Zuquan Hu:** Methodology, Investigation. **Jing Zhou:**

Investigation. Lina Liu: Investigation. **Wei Qiu:** Investigation. **Yuan-nong Ye:** Investigation. **Yi Jia:** Methodology, Investigation. **Shi Zhou:** Conceptualization, Formal analysis, Data curation, Funding acquisition. **Jinhua Long:** Conceptualization, Writing - review & editing, Supervision, Validation. **Zhu Zeng:** Conceptualization, Writing - review & editing, Supervision, Validation, Project administration, Funding acquisition.

Declaration of competing interest

The authors declare that they have no known competing financial interests or personal relationships that could have appeared to influence the work reported in this paper.

Acknowledgements

The authors thank the technical assistances from Y. Song and H. Min with immunofluorescence imaging.

This work was supported by the National Natural Science Foundation of China, China, 12132006, 31771014, 11762006, 31860262, 32160226, 21906036, the China Postdoctoral Science Foundation, China, 2019M653492, and the Guizhou Provincial Natural Science Foundation, China, 2019–2787, 2018-5779-54, 2018–1412, 2017–5718, 2016–5676, 2015–4021.

Appendix A. Supplementary data

Supplementary data to this article can be found online at <https://doi.org/10.1016/j.mtbio.2022.100224>.

References

- [1] C.A. Leifer, Dendritic cells in host response to biologic scaffolds, *Semin. Immunol.* 29 (2017) 41–48.
- [2] J.M. Anderson, A. Rodriguez, D.T. Chang, Foreign body reaction to biomaterials, *Semin. Immunol.* 20 (2008) 86–100.
- [3] P. Thevenot, W. Hu, L. Tang, Surface chemistry influences implant biocompatibility, *Curr. Trends Med. Chem.* 8 (2008) 270–280.
- [4] A. Nair, L. Tang, Influence of scaffold design on host immune and stem cell responses, *Semin. Immunol.* 29 (2017) 62–71.
- [5] N. Dekel, Y. Gnainsky, I. Granot, K. Racicot, G. Mor, The role of inflammation for a successful implantation, *Am. J. Reprod. Immunol.* 72 (2014) 141–147.
- [6] R.I. Litvinov, M. Pieters, Z. de Lange-Loots, J.W. Weisel, Fibrinogen and fibrin, *Subcell. Biochem.* 96 (2021) 471–501.
- [7] J.W. Weisel, R.I. Litvinov, Fibrin formation, structure and properties, *Subcell. Biochem.* 82 (2017) 405–456.
- [8] B.M. Tesar, D. Jiang, J. Liang, S.M. Palmer, P.W. Noble, D.R. Goldstein, The role of hyaluronan degradation products as innate alloimmune agonists, *Am. J. Transplant.* 6 (2006) 2622–2635.
- [9] G. Chan, D.J. Mooney, Ca²⁺ released from calcium alginate gels can promote inflammatory responses in vitro and in vivo, *Acta Biomater.* 9 (2013) 9281–9291.
- [10] P.M. Kou, Z. Schwartz, B.D. Boyan, J.E. Babensee, Dendritic cell responses to surface properties of clinical titanium surfaces, *Acta Biomater.* 7 (2011) 1354–1363.
- [11] S. Daneshmandi, S.P. Dibazar, S. Fateh, Effects of 3-dimensional culture conditions (collagen-chitosan nano-scaffolds) on maturation of dendritic cells and their capacity to interact with T-lymphocytes, *J. Immunot.* 13 (2016) 235–242.
- [12] Y.T. Tsai, J. Zhou, H. Weng, E.N. Tang, D.W. Baker, L. Tang, Optical imaging of fibrin deposition to elucidate participation of mast cells in foreign body responses, *Biomaterials* 35 (2014) 2089–2096.
- [13] A.C. Brown, T.H. Barker, Fibrin-based biomaterials: modulation of macroscopic properties through rational design at the molecular level, *Acta Biomater.* 10 (2014) 1502–1514.
- [14] N. Laurens, P. Koolwijk, M.P. de Maat, Fibrin structure and wound healing, *J. Thromb. Haemostasis* 4 (2006) 932–939.
- [15] M.A. Burkhardt, J. Waser, V. Milleret, I. Gerber, M.Y. Emmert, J. Fohlen, S.P. Hoerstrup, F. Schlottig, V. Vogel, Synergistic interactions of blood-borne immune cells, fibroblasts and extracellular matrix drive repair in an in vitro peri-implant wound healing model, *Sci. Rep.* 6 (2016) 21071.
- [16] R.I. Litvinov, J.W. Weisel, Fibrin mechanical properties and their structural origins, *Matrix Biol.* 60 (2017) 110–123.
- [17] G.W. Nelb, G.W. Kamykowski, J.D. Ferry, Rheology of fibrin clots. V. Shear modulus, creep, and creep recovery of fine unligated clots, *Biophys. Chem.* 13 (1981) 15–23.

- [18] M.R. Falvo, O.V. Gorkun, S.T. Lord, The molecular origins of the mechanical properties of fibrin, *Biophys. Chem.* 152 (2010) 15–20.
- [19] H. Kang, Q. Wen, P.A. Janney, J.X. Tang, E. Conti, F.C. MacKintosh, Nonlinear elasticity of stiff filament networks: strain stiffening, negative normal stress, and filament alignment in fibrin gels, *J. Phys. Chem. B* 113 (2009) 3799–3805.
- [20] L. Tang, T.A. Jennings, J.W. Eaton, Mast cells mediate acute inflammatory responses to implanted biomaterials, *Proc. Natl. Acad. Sci. U.S.A.* 95 (1998) 8841–8846.
- [21] J. Zdosek, J.W. Eaton, L. Tang, Histamine release and fibrinogen adsorption mediate acute inflammatory responses to biomaterial implants in humans, *J. Transl. Med.* 5 (2007) 31.
- [22] J.Y. Hsieh, T.D. Smith, V.S. Meli, T.N. Tran, E.L. Botvinick, W.F. Liu, Differential regulation of macrophage inflammatory activation by fibrin and fibrinogen, *Acta Biomater.* 47 (2017) 14–24.
- [23] J.M. Prasad, O.V. Gorkun, H. Raghu, S. Thornton, E.S. Mullins, J.S. Palumbo, Y.P. Ko, M. Höök, T. David, S.R. Coughlin, J.L. Degen, M.J. Flick, Mice expressing a mutant form of fibrinogen that cannot support fibrin formation exhibit compromised antimicrobial host defense, *Blood* 126 (17) (2015) 2047–2058.
- [24] G. Charras, E. Sahai, Physical influences of the extracellular environment on cell migration, *Nat. Rev. Mol. Cell Biol.* 15 (2014) 813–824.
- [25] V. Vogel, M. Sheetz, Local force and geometry sensing regulate cell functions, *Nat. Rev. Mol. Cell Biol.* 7 (2006) 265–275.
- [26] U. Haessler, M. Pisano, M. Wu, M.A. Swartz, Dendritic cell chemotaxis in 3D under defined chemokine gradients reveals differential response to ligands CCL21 and CCL19, *Proc. Natl. Acad. Sci. U.S.A.* 108 (2011) 5614–5619.
- [27] S.F.B. Mennens, M. Bolomini-Vittori, J. Weiden, B. Joosten, A. Cambi, K. van den Dries, Substrate stiffness influences phenotype and function of human antigen-presenting dendritic cells, *Sci. Rep.* 7 (2017) 17511.
- [28] T. Lämmermann, B.L. Bader, S.J. Monkley, T. Worbs, R. Wedlich-Söldner, K. Hirsch, M. Keller, R. Förster, D.R. Critchley, R. Fässler, M. Sixt, Rapid leukocyte migration by integrin-independent flowing and squeezing, *Nature* 453 (2008) 51–55.
- [29] J. Calmeiro, M. Carrascal, C. Gomes, A. Falcão, M.T. Cruz, B.M. Neves, Biomaterial-based platforms for in situ dendritic cell programming and their use in antitumor immunotherapy, *J. Immunother. Cancer* 7 (2019) 238.
- [30] S.K. Wculek, F.J. Cueto, A.M. Mujal, I. Melero, M.F. Krummel, D. Sancho, Dendritic cells in cancer immunology and immunotherapy, *Nat. Rev. Immunol.* 20 (1) (2020) 7–24.
- [31] F.J. Zhu, Y.L. Tong, Z.Y. Sheng, Y.M. Yao, Role of dendritic cells in the host response to biomaterials and their signaling pathways, *Acta Biomater.* 94 (2019) 132–144.
- [32] J. Constantino, C. Gomes, A. Falcão, B.M. Neves, M.T. Cruz, Dendritic cell-based immunotherapy: a basic review and recent advances, *Immunol. Res.* 65 (2017) 798–810.
- [33] Y. Liu, L. Xiao, K.I. Joo, B. Hu, J. Fang, P. Wang, *In situ* modulation of dendritic cells by injectable thermosensitive hydrogels for cancer vaccines in mice, *Biomacromolecules* 15 (2014) 3836–3845.
- [34] Z. Zeng, X. Liu, Y. Jiang, G. Wang, J. Zhan, J. Guo, W. Yao, D. Sun, W. Ka, Y. Tang, J. Tang, Z. Wen, S. Chien, Biophysical studies on the differentiation of human CD14⁺ monocytes into dendritic cells, *Cell Biochem. Biophys.* 45 (2006) 19–30.
- [35] X. Xu, X. Liu, J. Long, Z. Hu, Q. Zheng, C. Zhang, L. Li, Y. Wang, Y. Jia, W. Qiu, J. Zhou, W. Yao, Z. Zeng, Interleukin-10 reorganizes the cytoskeleton of mature dendritic cells leading to their impaired biophysical properties and motilities, *PLoS One* 12 (2017), e0172523.
- [36] T.L. Tang-Huau, E. Segura, Human *in vivo*-differentiated monocyte-derived dendritic cells, *Semin. Cell Dev. Biol.* 86 (2019) 44–49.
- [37] N. Romani, S. Gruner, D. Brang, E. Kämpgen, A. Lenz, B. Trockenbacher, G. Konwalinka, P.O. Fritsch, R.M. Steinman, G. Schuler, Proliferating dendritic cell progenitors in human blood, *J. Exp. Med.* 180 (1) (1994) 83–93.
- [38] L. Rakers, D. Grill, A.L.L. Matos, S. Wulff, D. Wang, J. Börgel, M. Körsgen, H.F. Arlinghaus, H.J. Galla, V. Gerke, F. Glorius, Addressable cholesterol analogs for live imaging of cellular membranes, *Cell Chem. Biol.* 25 (2018) 952–961.
- [39] J. Park, J.E. Babensee, Differential functional effects of biomaterials on dendritic cell maturation, *Acta Biomater.* 8 (2012) 3606–3617.
- [40] A.D. Friedman, O. Dan, J.A. Drazba, R.R. Lorenz, M. Strome, Quantitative analysis of OX62-positive dendritic cell distribution in the rat laryngeal complex, *Ann. Otol. Rhinol. Laryngol.* 116 (2007) 449–456.
- [41] O.R. Oakley, H. Kim, I. El-Amouri, P.C. Lin, J. Cho, M. Bani-Ahmad, C. Ko, Periovarial leukocyte infiltration in the rat ovary, *Endocrinology* 151 (2010) 4551–4559.
- [42] W. Yang, Y. Tao, Y. Wu, X. Zhao, W. Ye, D. Zhao, L. Fu, C. Tian, J. Yang, F. He, L. Tang, Neutrophils promote the development of reparative macrophages mediated by ROS to orchestrate liver repair, *Nat. Commun.* 10 (2019) 1076.
- [43] J. Toyjanova, E. Flores-Cortez, J.S. Reichner, C. Franck, Matrix confinement plays a pivotal role in regulating neutrophil-generated tractions, speed, and integrin utilization, *J. Biol. Chem.* 290 (2015) 3752–3763.
- [44] A. Marki, K. Buscher, C. Lorenzini, M. Meyer, R. Saigusa, Z. Fan, Y.T. Yeh, N. Hartmann, J.M. Dan, W.B. Kiesses, G.J. Golden, R. Ganesan, H. Winkels, M. Orechioni, S. McArdle, Z. Mikulski, Y. Altman, J. Bui, M. Kronenberg, S. Chien, J.D. Esko, V. Nizet, D. Smalley, J. Roth, K. Ley, Elongated neutrophil-derived structures are blood-borne microparticles formed by rolling neutrophils during sepsis, *J. Exp. Med.* 218 (2021), e20200551.
- [45] A. Leithner, A. Eichner, J. Müller, A. Reversat, M. Brown, J. Schwarz, J. Merrin, D.J. de Gorter, F. Schur, J. Bayerl, I. de Vries, S. Wieser, R. Hauschild, F.P. Lai, M. Moser, D. Kerjaschki, K. Rottner, J.V. Small, T.E. Stradal, M. Sixt, Diversified actin protrusions promote environmental exploration but are dispensable for locomotion of leukocytes, *Nat. Cell Biol.* 18 (2016) 1253–1259.
- [46] M.M. Ménager, D.R. Littman, Actin dynamics regulates dendritic cell-mediated transfer of HIV-1 to T cells, *Cell* 164 (2016) 695–709.
- [47] W.A. Comrie, S. Li, S. Boyle, J.K. Burkhardt, The dendritic cell cytoskeleton promotes T cell adhesion and activation by constraining ICAM-1 mobility, *J. Cell Biol.* 208 (2015) 457–473.
- [48] P. Vargas, P. Maiuri, M. Bretou, P.J. Sáez, P. Pierobon, M. Maurin, M. Chabaud, D. Lankar, D. Obino, E. Terriac, M. Raab, H.R. Thiam, T. Brocker, S.M. Kitchen-Goosen, A.S. Alberts, P. Sunareni, S. Xia, R. Li, R. Voituriez, M. Piel, A.M. Lennon-Duménil, Innate control of actin nucleation determines two distinct migration behaviours in dendritic cells, *Nat. Cell Biol.* 18 (2016) 43–53.
- [49] C. Reis e Sousa, Dendritic cells in a mature age, *Nat. Rev. Immunol.* 6 (2006) 476–483.
- [50] M. Butler, A.S. Morel, W.J. Jordan, E. Eren, S. Hue, R.E. Shrimpton, M.A. Ritter, Altered expression and endocytic function of CD205 in human dendritic cells, and detection of a CD205-DCL-1 fusion protein upon dendritic cell maturation, *Immunology* 120 (2007) 362–371.
- [51] S. Celli, Z. Garcia, H. Beuneeu, P. Bousso, Decoding the dynamics of T cell-dendritic cell interactions *in vivo*, *Immunol. Rev.* 221 (2008) 182–187.
- [52] S. Hugues, Dynamics of dendritic cell-T cell interactions: a role in T cell outcome, *Semin. Immunopathol* 32 (2010) 227–238.
- [53] T.S. Lim, J.K. Goh, A. Mortellaro, C.T. Lim, G.J. Hämmerling, P. Ricciardi-Castagnoli, CD80 and CD86 differentially regulate mechanical interactions of T-cells with antigen-presenting dendritic cells and B-cells, *PLoS One* 7 (2012), e45185.
- [54] C.V. Jakubczik, G.J. Randolph, P.M. Henson, Monocyte differentiation and antigen-presenting functions, *Nat. Rev. Immunol.* 17 (2017) 349–362.
- [55] I.L. Tourkova, G.V. Shurin, S. Wei, M.R. Shurin, Small rho GTPases mediate tumor-induced inhibition of endocytic activity of dendritic cells, *J. Immunol.* 178 (2007) 7787–7793.
- [56] M. Bros, K. Haas, L. Moll, S. Grabbe, RhoA as a key regulator of innate and adaptive immunity, *Cells* 8 (2019) 733.
- [57] C.A. Swetman, Y. Leverrier, R. Garg, C.H. Gan, A.J. Ridley, D.R. Katz, B.M. Chain, Extension, retraction and contraction in the formation of a dendritic cell dendrite: distinct roles for Rho GTPases, *Eur. J. Immunol.* 32 (2002) 2074–2083.
- [58] J.Q. Wang, L. Mao, The ERK pathway: molecular mechanisms and treatment of depression, *Mol. Neurobiol.* 56 (2019) 6197–6205.
- [59] J.M. Yang, S. Bhattacharya, H. West-Foyle, C.F. Hung, T.C. Wu, P.A. Iglesias, C.H. Huang, Integrating chemical and mechanical signals through dynamic coupling between cellular protrusions and pulsed ERK activation, *Nat. Commun.* 9 (2018) 4673.
- [60] A. Rajesh, G. Stuart, N. Real, J. Ahn, A. Tschirley, L. Wise, M. Hibma, Depletion of langerin⁺ cells enhances cutaneous wound healing, *Immunology* 160 (2020) 366–381.
- [61] A.C. Bendell, N. Anderson, D. Blumenthal, E.K. Williamson, C.S. Chen, J.K. Burkhardt, D.A. Hammer, Motile dendritic cells sense and respond to substrate geometry, *Ann. Biomed. Eng.* 46 (2018) 1348–1361.
- [62] D.E. Discher, P. Janmey, Y.L. Wang, Tissue cells feel and respond to the stiffness of their substrate, *Science* 310 (2005) 1139–1143.
- [63] M. Chakraborty, K. Chu, A. Shrestha, X.S. Revelo, X. Zhang, M.J. Gold, S. Khan, M. Lee, C. Huang, M. Akbari, F. Barrow, Y.T. Chan, H. Lei, N.K. Kotoulas, J. Jovel, C. Pastrello, M. Kotlyar, C. Goh, E. Michelakis, X. Clemente-Casares, P.S. Ohashi, E.G. Engleman, S. Winer, I. Jurisica, S. Tsai, D.A. Winer, Mechanical stiffness controls dendritic cell metabolism and function, *Cell Rep.* 34 (2021) 108609.
- [64] R. Sridharan, B. Cavanagh, A.R. Cameron, D.J. Kelly, F.J. O'Brien, Material stiffness influences the polarization state, function and migration mode of macrophages, *Acta Biomater.* 89 (2019) 47–59.
- [65] M.L. Heuzé, P. Vargas, M. Chabaud, M. Le Berre, Y.J. Liu, O. Collin, P. Solanes, R. Voituriez, M. Piel, A.M. Lennon-Duménil, Migration of dendritic cells: physical principles, molecular mechanisms, and functional implications, *Immunol. Rev.* 256 (2013) 240–254.
- [66] W.Y. Wang, C.D. Davidson, D. Lin, B.M. Baker, Actomyosin contractility-dependent matrix stretch and recoil induces rapid cell migration, *Nat. Commun.* 10 (2019) 1186.
- [67] M. Jaspers, S.L. Vaessen, P. van Schayik, D. Voerman, A.E. Rowan, P.H.J. Kouwer, Nonlinear mechanics of hybrid polymer networks that mimic the complex mechanical environment of cells, *Nat. Commun.* 8 (2017) 15478.
- [68] M. Huse, Mechanical forces in the immune system, *Nat. Rev. Immunol.* 17 (2017) 679–690.
- [69] S.A. Freeman, S. Grinstein, Phagocytosis: receptors, signal integration, and the cytoskeleton, *Immunol. Rev.* 262 (2014) 193–215.
- [70] T.A. Masters, B. Pontes, V. Viasnoff, Y. Li, N.C. Gauthier, Plasma membrane tension orchestrates membrane trafficking, cytoskeletal remodeling, and biochemical signaling during phagocytosis, *Proc. Natl. Acad. Sci. U.S.A.* 110 (2013) 11875–11880.
- [71] T. Worbs, S.I. Hammerschmidt, R. Förster, Dendritic cell migration in health and disease, *Nat. Rev. Immunol.* 17 (2017) 30–48.

- [72] L. Tiberio, A. Del Prete, T. Schioppa, F. Sozio, D. Bosisio, S. Sozzani, Chemokine and chemotactic signals in dendritic cell migration, *Cell. Mol. Immunol.* 15 (2018) 346–352.
- [73] K.F. Tolias, J.G. Duman, K. Um, Control of synapse development and plasticity by Rho GTPase regulatory proteins, *Prog. Neurobiol.* 94 (2011) 133–148.
- [74] R. Gazzeri, C. Fiore, M. Galarza, Role of EVICEL fibrin sealant to assist hemostasis in cranial and spinal epidural space: a neurosurgical clinical study, *Surg. Technol. Int.* 26 (2015) 364–369.
- [75] W. Bensaïd, J.T. Triffitt, C. Blanchat, K. Oudina, L. Sedel, H. Petite, A biodegradable fibrin scaffold for mesenchymal stem cell transplantation, *Biomaterials* 24 (2003) 2497–2502.
- [76] M.E. Davis, P.C. Hsieh, A.J. Grodzinsky, R.T. Lee, Custom design of the cardiac microenvironment with biomaterials, *Circ. Res.* 97 (2005) 8–15.
- [77] E. Ahmad, M.T. Fatima, M. Hoque, M. Owais, M. Saleemuddin, Fibrin matrices: the versatile therapeutic delivery systems, *Int. J. Biol. Macromol.* 81 (2015) 121–136.
- [78] J. Xu, P. Zanvit, L. Hu, P.Y. Tseng, N. Liu, F. Wang, O. Liu, D. Zhang, W. Jin, N. Guo, Y. Han, J. Yin, A. Cain, M.A. Hoon, S. Wang, W. Chen, The cytokine TGF- β induces interleukin-31 expression from dermal dendritic cells to activate sensory neurons and stimulate wound itching, *Immunity* 53 (2020) 371–383.